NASA/TM-2005-213254

Error Due to Wing Bending in Single-Camera Photogrammetric Technique

Alpheus W. Burner, Jr. and Danny A. Barrows
Langley Research Center, Hampton, Virginia

May 2005

The NASA STI Program Office . . . in Profile

Since its founding, NASA has been dedicated to the advancement of aeronautics and space science. The NASA Scientific and Technical Information (STI) Program Office plays a key part in helping NASA maintain this important role.

The NASA STI Program Office is operated by Langley Research Center, the lead center for NASA's scientific and technical information. The NASA STI Program Office provides access to the NASA STI Database, the largest collection of aeronautical and space science STI in the world. The Program Office is also NASA's institutional mechanism for disseminating the results of its research and development activities. These results are published by NASA in the NASA STI Report Series, which includes the following report types:

- TECHNICAL PUBLICATION. Reports of completed research or a major significant phase of research that present the results of NASA programs and include extensive data or theoretical analysis. Includes compilations of significant scientific and technical data and information deemed to be of continuing reference value. NASA counterpart of peer-reviewed formal professional papers, but having less stringent limitations on manuscript length and extent of graphic presentations.

- TECHNICAL MEMORANDUM. Scientific and technical findings that are preliminary or of specialized interest, e.g., quick release reports, working papers, and bibliographies that contain minimal annotation. Does not contain extensive analysis.

- CONTRACTOR REPORT. Scientific and technical findings by NASA-sponsored contractors and grantees.

- CONFERENCE PUBLICATION. Collected papers from scientific and technical conferences, symposia, seminars, or other meetings sponsored or co-sponsored by NASA.

- SPECIAL PUBLICATION. Scientific, technical, or historical information from NASA programs, projects, and missions, often concerned with subjects having substantial public interest.

- TECHNICAL TRANSLATION. English-language translations of foreign scientific and technical material pertinent to NASA's mission.

Specialized services that complement the STI Program Office's diverse offerings include creating custom thesauri, building customized databases, organizing and publishing research results ... even providing videos.

For more information about the NASA STI Program Office, see the following:

- Access the NASA STI Program Home Page at ***http://www.sti.nasa.gov***

- E-mail your question via the Internet to help@sti.nasa.gov

- Fax your question to the NASA STI Help Desk at (301) 621-0134

- Phone the NASA STI Help Desk at (301) 621-0390

- Write to:
  NASA STI Help Desk
  NASA Center for AeroSpace Information
  7121 Standard Drive
  Hanover, MD 21076-1320

NASA/TM-2005-213254

Error Due to Wing Bending in Single-Camera Photogrammetric Technique

Alpheus W. Burner, Jr. and Danny A. Barrows
Langley Research Center, Hampton, Virginia

National Aeronautics and
Space Administration

Langley Research Center
Hampton, Virginia 23681-2199

May 2005

Available from:

NASA Center for AeroSpace Information (CASI)
7121 Standard Drive
Hanover, MD 21076-1320
(301) 621-0390

National Technical Information Service (NTIS)
5285 Port Royal Road
Springfield, VA 22161-2171
(703) 605-6000

Abstract

The error due to wing bending introduced into single-camera photogrammetric computations used for the determination of wing twist or control surface angular deformation is described. It is shown that the error due to wing bending when determining main wing element-induced twist is typically less than 0.05° at the wing tip and may not warrant additonal correction. It is also shown that the angular error in control surface deformation due to bending can be as large as 1° or more if the control surface is at a large deflection angle compared to the main wing element. A correction procedure suitable for control surface measurements is presented. Simulations of the error based on typical wind tunnel measurement geometry, and results from a controlled experimental test in the test section of the National Transonic Facility (NTF) are presented to confirm the validity of the method used for correction of control surface photogrammetric deformation data. An example of a leading edge (LE) slat measurement is presented to illustrate the error due to wing bending and its correction.

Introduction

A single-camera, single-view photogrammetric technique has been used at a number of NASA wind tunnels (ref. 1) to measure flow-induced wing twist and control surface deformation. The technique is often referred to as the videogrammetric model deformation (VMD) technique because video-rate cameras, combined with automated image processing, are used in addition to single-camera, single-view photogrammetry data reduction. A requirement when using the technique is that one of the three spatial coordinates must be known to allow for a single-camera, single-view photogrammetric solution. For pitch-sweep tunnel tests without roll, the known coordinate is most often the spanwise locations of the targets, which remain constant as the model is pitched without flow. This condition is not the case for wind-on testing, however, because flow-induced wing bending causes slight changes in the spanwise location of targets. The effects of this error in the known spanwise coordinates on the measurement of flow-induced aeroelastic wing twist were first discussed in reference 2, in which it was noted that the error was expected to be small for targets at a given spanwise location since the targets experience similar bending and hence have similar biases, which largely cancel in the differencing that is used in the induced twist angle computation. This bias error is discussed in more detail in reference 3, in which some approximate formulas are presented to estimate the shift in the spanwise coordinate as a function of the bending. A procedure is presented in reference 3, in which the measured bending without correction is used to estimate the spanwise shift that can then be used in an iterative photogrammetric computation to apply a correction to the measured deflection; however, the functional form of the bending and the inboard location of zero bending must be known. Reference 3 states that only one or two iterations are necessary for most applications. This paper further discusses this bias error and its correction and contrasts the relatively large angular error (compared to the main wing element induced twist error) that may arise for control surfaces set at large deflection angles. A new correction procedure applicable to control surfaces is presented that is based only on the invariance of the length between targets during bending. Questionable leading-edge (LE) slat angular deformation data during testing at the National Transonic Facility (NTF) prompted the effort reported here. The original uncorrected slat deformation data for that test indicated a downward deflection (instead of upward as expected) of the LE slat of over 1° as positive aeroelastic loading occurred. This physically suspect result prompted this investigation of bias errors that might cause such a result for deflected control surfaces, while at the same time causing little error to main wing data.

Basis of Photogrammetric Error Due to Wing Bending

The error due to wing bending occurs because of the constraint on the arc length of the main wing element when it is undergoing flow-induced deformation. Thus, for instance, as the wing tip moves upward during positive loading due to aerodynamic loads, the wing tip (and proportionally the whole wing) moves slightly toward the fuselage. In the usual single-camera photogrammetric data reduction solution, this shift in the spanwise coordinate, which is assumed to be known and constant, is ignored. Thus, a bias error is introduced that is proportional to the amount of deflection, or wing bending. This spanwise shift can be simply illustrated with the rotation of a flat plate of length L about a fixed point. In a 2-D coordinate system, with Z up and Y horizontal, the Y coordinate of a point at the tip of the flat plate of length L, as it is rotated by an angle ω, is given by $L \cos \omega$ so that the shift in the assumed *known* Y coordinate of the tip is given by $L\ (1 - \cos \omega)$. For example, for a length L of 30 in. and a linear tip deflection of 1 in., the angle of rotation ω would be $\sin^{-1}(1/30) = 1.91°$, giving a shift in Y at the tip toward the model body equal to 0.017 in. Thus, the correct Y value to use for a single-camera photogrammetric solution for a target at the tip undergoing linear bending of 1 in. would be 29.983 instead of 30. This effect is emphasized in figure 1 where, in addition to the flat plate, second- through fourth-order polynomial curves with basic functional form $Z = Y^2$, Y^3, and Y^4 are also presented with the constraint that the arc length must be maintained at unity as the bending occurs and that the projected bending at $Y = 1$ is unity. The constrained arc length of unity is depicted (fig. 1) in red (heavy line) for each of the polynomials. The shift in the Y coordinate at the tip for the second-order curve is depicted in figure 1 as well (indicated as Y_{shift}). The arc length computations for the second- through fourth-order curves are not simple trigonometric relations but rather are arc length integral relationships (see appendix A). Note that figure 1 is used to emphasize the effect and actually represents much larger relative deflection than is typically observed for wing bending in wind tunnel testing. Maximum wing tip bending is more typically on the order of 1/30 of the spanwise coordinate Y instead of the relatively large values of figure 1. Table 1 contrasts the Y values (represented by Y_1) for constant arc length $s = 1$ for first- through fourth-order bending (order appears in column 1), all with the functional form of the bending having a deflection of unity at the maximum semispan L. The Y_1 values to maintain an arc length equal to L = Unity and $L = 30$ are given, as well as the computed arc length s at $Y_1 = 1$ and $Y_1 = 30$. Columns 2 and 3 of table 1 correspond to figure 1 whereas columns 4 and 5 correspond to a more typical transonic case of around 1-in. maximum deflection at a semispan of 30 in. Columns 3 and 5 illustrate the error in the spanwise location that is experienced when assuming that a target undergoing bending only translates in Z, not Y. Columns 2 and 4 illustrate the shift in the *assumed* Y coordinate used in the single-camera photogrammetric computation. For example, the shift for second-order bending with an undeflected semispan of 30 in. is given by 30 – 29.9778 = 0.0222 in. toward the model body.

Table 1. Y_1 and Arc Length s at Unity and 30

Order	Y_1 ($s = 1$)	s ($Y_1 = 1$)	Y_1 ($s = 30$)	s ($Y_1 = 30$)
1	0.7071	1.4142	29.9833	30.0167
2	0.7639	1.4789	29.9778	30.0222
3	0.7907	1.5479	29.9702	30.0300
4	0.8105	1.6002	29.9623	30.0380

Most of the flow-induced twist that occurs from wing bending arises because target pairs located on the main wing element are located at constant semispan, not necessarily constant distance along the elastic axis (fig. 2). Assuming a rearward swept wing, as the wing bends upward under a positive wing load, the trailing edge (TE) target is located farther from the point of zero bending than the LE target, which leads to the commonly observed negative-induced twist (washout) associated with an upward bending of a rearward swept wing. This effect also means that the TE and LE targets are displaced slightly along the elastic axis of the wing, as depicted in figure 3. In figure 3, target 1 represents the LE target located at a value of 0.97 and target 2 represents the TE target located at 1.00 (tip). As the wing bends, the two targets experience similar *Y* shifts of around 0.25. The initial difference in *Y* between the two targets of 0.030 reduces to 0.017 after undergoing second-order bending. Thus, the bias errors of the two targets are similar and tend to largely cancel with the subtraction inherent in the angular calculations. The bias error in angle that is left is generally less than 0.1°. Figure 3 exaggerates the effect for illustration. A simulation of this effect, better scaled to typical wind tunnel results, is presented in the next section of this paper to quantify the magnitude of the effect in both angle and spatial coordinates as well as the suitability of an iterative correction procedure.

The angular error in determining main wing element flow-induced wing twist may, in many cases, not be a significant source of error (as will be illustrated in more detail later). However, the angular error can be significant for control surfaces initially set at relatively large angles to the main wing. This significant error occurs because targets at the extremities of deflected control surfaces can be displaced significantly in *Z* compared to the *Z*-separation of main wing targets as the wing undergoes bending due to aerodynamically induced loading. Tilt of the control surface toward the model body due to aeroelastic loading will tend to separate the targets on the deflected control surface in the *Y*-direction much more than for the main wing element targets, leading to increased *Y*-shift error for the deflected control surface. This effect is exaggerated with the simple sketch shown in figure 4. As the control surface follows the bending of the wing, there can be significant differences in *Y* between a target near the main wing element (target 1 in fig. 4) and a target at the extreme of the deflected control surface (target 2). Before bending occurs, the targets on the control surface of the simple example of figure 4 are at equal *Y*-coordinates of 1, with target 2 at the extremity of the control surface located 0.1 unit below target 1 on the undeformed wing. After bending, targets 1 and 2 are displaced significantly more in *Y* than the two targets on the main wing element example of figure 3 due to the tilt of the control surface as it follows the bending of the main wing. Examples of the magnitude and a new method of correction of this bias error for highly deflected control surfaces are presented later, after a discussion of the relatively small photogrammetric errors of main wing element targets presented in the next section.

Photogrammetric Error for Main Wing Element

The single-camera photogrammetric error for main wing element targets was assessed by simulation using a camera geometry and lens focal length similar to that used for transonic testing. The following camera parameters listed in table 2 were used in the simulation. The symbols are defined in appendix B.

The analyses were conducted for a target pair separated by 1 in. and located 30 in. from the position of zero bending, representing two targets that might lie near the wing tip. The coordinate *X* is in the flow direction, *Y* is along the span, and *Z* is up. The second-order bending for one of the targets was fixed at 1 in. The second-order deflection of the other target was varied ±0.1 in. (corresponding to ±5.7° induced twist) to assess the error in angle and in the computation of *X* and *Z*, in addition to the error in the assumed *Y* value caused by bending. The collinearity equations (appendix B) were used to compute exact image plane coordinates given the camera parameters in table 2, the deflected *Z* values, and the shifted *Y* values (due to second-order bending). The single-camera photogrammetric computation outlined in appendix B was then used to compute *X* and *Z* by using the initial value of *Y* (30 in.) without

Table 2. Camera Parameters

Parameter	Value	Units
c	26.3	mm
x_p	−0.23	mm
y_p	0.33	mm
ω	61.6	deg
ϕ	0.2	deg
κ	−90.8	deg
X_c	0.1	in.
Y_c	−55.2	in.
Z_c	34.5	in.

compensating for the shift in Y due to bending. Angles were computed as the negative of the arctangent in the XZ plane of the single-camera computed X and Z coordinates of the two targets. The difference in the angle from no load to bending was taken to be the induced twist. The error in the twist computation, as a function of the simulated twist angle (based on the varying deflection of the second target), is plotted in figure 5 over a range of ±6°, which is about twice the maximum values typically seen in transonic testing. The maximum angular error from the plot is noted to be less than 0.1°. The angular error is approximately −1.5 percent of the twist angle, which for angles below 3° is less than the generally accepted noise floor for induced twist of 0.05°. The induced twist is slightly underestimated if the Y shift due to bending is ignored. The angular error scales directly with the deflection. In other words, the photogrammetric error, when ignoring the Y shift due to bending at 0.5-in. deflection at a semispan of 30 in., is about half of the error found at a 1-in. deflection for the same semispan. Additional simulations also show that the magnitude of the angular error is relatively independent of the spacing of the targets because the error in Z that leads to the angular error is relatively independent of the X location of the targets. Thus, the percentage error due to bending improves with target spacing.

The error in X, Y, and Z is presented in figure 6 over the same twist angle range. The X error is small (a few thousandths of an inch) and nearly constant. The Z error is a little larger but is still less than 0.01 in. The Z error has a slight negative bias (−0.007 in.) due to the view angle of the camera with respect to the XY plane. If the targets are closer to the camera than assumed, as occurs when subjected to bending (with the camera viewing the farthest wing looking over the model body), the single-camera solution will lead to a slight negative bias in Z. The Y-error shown in figure 6 is just the difference in the assumed 30-in. value for Y and the actual value of Y of the targets due to second-order bending. A shift of about 0.022 in. toward the fuselage is noted for 1-in. deflection of second-order bending at a Y of 30 in. The Y-error varies slightly about that value as the deflection of the second target varies about 1-in.

The iterative procedure of reference 3 is next used to estimate the correct value of Y for use in the single-camera solution. New X, Z coordinates are then computed from the single-camera solution with the partially corrected Y value as input. This procedure is then repeated one more time. The error in the twist and the spatial coordinate computations after this iterative correction procedure is shown in figures 7 and 8. The error in twist after the iterative correction is then shown to be less than 0.001°. The errors in the spatial coordinates are shown to be generally less than 0.0001 in. The additional errors introduced into this iterative correction procedure when the location of zero bending Y_0 is not known accurately are shown in figure 9 for twist and in figure 10 for X, Y, and Z. The error in the twist computation generally is still less than 0.02°, and the spatial errors are generally less than 0.01 in., even when the point of zero bending is only known to ±10 in.

Although the simulations previously discussed give a sense of the magnitude and dependence of the error caused by ignoring the *Y*-shift due to bending, they do not take into account the sweep of the wing to simplify the analyses. For this reason, an additional simulation was conducted to assess what additional effect the wing sweep might have on the error due to bending. As discussed earlier, the location of targets at the same semispan location introduces a separation along the elastic axis of a swept wing (fig. 2). Assume there are two targets at a semispan of 30 in. separated by *d* inches, with one target located near the TE and one located near the LE of a wing with a sweep of 30°. Second-order bending is applied with the deflection of the TE target set at 1 in. The two targets will have slightly different *Y* shifts because the LE target is closer to the point of zero bending (for a rearward swept wing) and hence is deflected less than the TE target, as discussed for figure 3. For the simulation of wing sweep, the collinearity equations are used to compute exact image plane coordinates given the 3-D spatial coordinates of each target, taking into account the *Y* shift due to second-order bending. A single-camera photogrammetric solution is used to compute *X*, *Z* spatial coordinates from the exact image plane coordinates by ignoring the *Y*-shift due to bending in order to compare the angle computed (ignoring the shift) with the exact angle. The angle found when the *Y*-shift is ignored is underestimated by slightly less than 1 percent, nearly independently of the target separation *d* and twist, as seen in figure 11, where *d* is varied from near zero to 4 in. (with a corresponding variation in simulated twist of near 0° to −6°). For a separation *d* of 2 in., this shift along the elastic axis produces a twist in the streamwise direction of −3.20° for a nominal deflection of 1 in. for the TE target. When ignoring the shift in the *Y* coordinate, the single-camera photogrammetry solution yields −3.17°. The previous simulations should adequately describe the nature of the main wing error, even without including wing sweep.

Note that for this correction of the simulation data, the functional form of the bending was known exactly, as well as the location of zero bending. Also note that the corrections here used exact image plane coordinates and exact camera parameters. For typical wind tunnel measurements, it is expected that image plane errors coupled with camera parameter errors, along with flow-induced errors, may make this iterative correction procedure less than robust and may not be warranted because of the small value of the correction for all but the most outboard wing locations. At the generally accepted level of accuracy for angular wing deformation of about 0.05°, along with the uncertainty in image plane coordinates and camera parameters, it may not currently be advantageous to correct for the small *Y*-shift error due to bending for main wing element targets. However, as accuracy improves and requirements for measured flow-induced changes in wing twist become more demanding, the iterative correction procedure discussed here should be revisited to assess its value and applicability during wind tunnel testing that uses the single-camera, single-view photogrammetric approach.

Photogrammetric Error for Highly Deflected Control Surfaces

Unlike the *Y*-shift error due to bending experienced by main wing element targets, the bending error of targets on highly deflected control surfaces can be relatively large, as pointed out previously and illustrated with the geometry of figure 4. A simulation based on a standard wind tunnel camera geometry was conducted to assess the magnitude of this error and investigate a possible correction scheme. The simple case of linear bending was used to simplify the analysis. Since it is the tilt angle in the spanwise direction between the targets at the leading and trailing edges of the control surface that largely determines the error, the functional form of the bending is not as critical. The correction technique that is presented in the next section is not dependent on the functional form of the bending. Once the corrected *Y* coordinates are determined, a local spanwise tilt angle is computed from the angle in the *YZ* plane.

A set of *X*, *Y*, and *Z* coordinates for four targets is used for the simulation. The two targets on the main wing element are at the same initial *Z* value before bending. The other two targets on the LE control surface, which is deflected downward at −25° from the main wing element, are displaced in Z by 0.36 in. from each other. During the simulated wing bending, the deflection angle of the control surface to the main wing element is held constant. In other words, there should be no change in the computed control surface deflection relative to the main wing as bending is simulated, which is equivalent to keeping the control surface plane of tilt perpendicular to the main wing where they intersect (fig. 4). Any change in the deflection angle of the control surface is a measure of the error in determining the deflected angle.

A plot of the four target locations before deflection (at $\omega = 0°$, indicated with circles) and after the maximum upward vertical deflection (at $\omega = -2°$, indicated with squares) is shown in figure 12. A negative value of ω causes an upward linear deflection, given the coordinate system and camera location used for this simulation. Before bending, all four targets are at the same Y value. After bending (linear for this case), the two targets located on the main wing element (with the same initial value of Z) shift identical amounts in Y; whereas, the two targets on the LE control surface (initially separated in Z) are displaced in Y after bending (as illustrated in fig. 13) by 0.013 in. Note that in figure 13, the main wing targets have the same Z values before and after deflection so they are indicated with 1 symbol each. In figure 14, a conformal transformation of the Y and Z coordinates was used to transform the undeflected coordinates through a spanwise tilt angle of −2° (designated ω here since the rotation is about the X-axis). The center of rotation was offset by 24 in. from the location of the control surface targets, which were assumed to initially be at the same value of Y before linear bending. The Z deflection at the spanwise location of the targets was 0.84 in. upward for the maximum −2° linear bending (fig. 12). The values of spanwise rotation and Z deflection were chosen to roughly simulate the wing bending experienced at the measurement location of the LE slat during a recent wind tunnel test. The transformed Y, Z coordinates were used to create exact image plane data through the collinearity equations in a similar manner to the ones previously discussed. Camera parameters used for the simulation were identical to those used during an actual LE slat measurement at the NTF. The single-camera photogrammetric data reduction procedure (appendix B) was used to compute X and Z from the exact image plane coordinates, ignoring the Y shift due to bending. The difference between the angle of the two targets on the control surface and the angle of the two targets on the main wing element is then computed and compared to the set value of −25°. Any variation is taken to be the error in the computed angle.

The error in the angle of the main wing and the error in the angle of the LE control surface set at −25° as linear bending is applied (which moves the wing tip upward as the rotation angle changes from 0° to −2°) are depicted in figure 15. For this simple simulation, there is no angular error for the main wing element because the Y shift for both targets is identical, producing equal bias errors for both targets. Thus, the differencing that occurs in the arctangent computation in the XZ plane yields zero, even though the scale is slightly off due to the Y shift error (the X and Z values of the two wing targets are slightly in error due to this error in scale). Unlike the wing targets, however, the error in the computation of the angle of the LE control surface varies almost linearly to −1.31° at the maximum rotation of −2°, which is equivalent to an erroneous inference that the angle of the control surface has been deflected downward from −25° by this amount to a new angle of −26.31°. In other words, the leading edge of the control surface would appear to be deflected downward by 1.31°. Unlike the errors discussed in the previous section for the main wing, the magnitude of the angular error for the control surface is much more significant; thus, a method of correction of this error is highly desirable.

Correction Method for Control Surfaces

Since the scale of the photogrammetric computation is in error, it might be expected that the computation of length between targets based on single-camera photogrammetry would be affected as well. Numbering the targets 1 through 4 from LE (on the control surface) to TE (on the wing), the errors in the length between targets 1 and 4, 2 and 4, and 3 and 4 are depicted in figure 16. The error in the computed length is relatively small (<0.017-in. maximum) but is nearly linear and very systematic. As might be expected, the error increases with the magnitude of the length between targets (targets 1 and 4 have the largest separation). The systematic nature of the computed lengths when wing bending bias error is present led naturally to the basis of the new correction scheme suitable for control surfaces, which is to determine the shift in *Y* that will minimize the error in the computed lengths between targets. An advantage of this technique is that the functional form of the bending and the location where the bending goes to zero do not have to be known. With this correction technique, the local spanwise angle of the targets in the *YZ* plane can also be determined given the newly corrected *Y* coordinates.

The new correction procedure consists of the following steps. The lengths between several target pairs are first computed for the undeflected reference condition based on single-camera photogrammetry. This reference condition would normally be wind-off at the same model pitch angle (and possibly at the same temperature and pressure). Note that before loading (deflection) occurs, single-camera photogrammetry does not suffer from the bending bias error and should yield an adequate measure of the lengths. Also, by using the wind-off photogrammetry calculations of lengths as reference, any bias errors common to both wind-off and wind-on will tend to cancel. For this simulation, the lengths between target 4 and each of the targets (1, 2, and 3) are computed. For each of the simulated linear bending cases from 0° to −2°, the lengths between these same target pairs are then computed from single-camera photogrammetry by using the initial value of *Y* before bending is initiated. The undeflected reference lengths are then subtracted to determine the change in the apparent length computations. Single-camera photogrammetry is then repeated with *Y* incremented, for instance, by 0.01 in. for targets 1, 2, and 3. The differences in the three lengths from the undeflected are then recomputed. The slope and intercept of the change in *Y* versus the change in length between undeflected and deflected are then computed. The intercept is the initial estimate of the shift in *Y* necessary to eliminate the difference between the deflected length and undeflected reference length of each of the three target pairs. A small increment can then be both added and subtracted from the initial estimate of the shift in *Y* and the intercept and slope recomputed for a possible improved estimate. This process is repeated one more time, if necessary, with a smaller increment to arrive at the final value of the shift in *Y* to eliminate the difference between the lengths for the deflected and the undeflected reference. The single-camera photogrammetric solution is then repeated one final time with the latest estimate of corrected *Y* before computing the arctangent of the angle in the *XZ* plane. The negative of the arctangent of the slope of the shifted *Y* values versus *Z* for the four targets yields the amount of spanwise rotation ω. The final angle determination then consists of dividing the difference in the *Z* values between appropriate target pairs by the cosine of the computed ω before dividing by the *X* differences and computing the arctangent of the resultant. This last scaling of the *Z* values by the inverse of $\cos(\omega)$ is to account for the tilt of the control surface in the *YZ* plane as bending occurs (illustrated with fig. 4).

The residual errors in the angles of the LE control surface and the main wing are shown in figure 17 as a function of ω. The maximum control surface angular error residual is less than 0.05° or about 3.5 percent of the angular error before correction. The angular error of the main wing is actually increased slightly to a little more than 0.02°. The error in the computed value of ω from the correction procedure is presented in figure 18. The spanwise tilt angle ω is found to within 0.11° at the maximum tilt angle of −2°, or within about 5 percent.

Wind-Off Angle Test in National Transonic Facility Test Section

A wind-off, open test section evaluation was conducted in the NTF to assess the effects of spanwise angular motion of LE control surface and main wing targets. The test incorporated a target fixture that simulated two targets on the main wing and two targets on the LE control surface (fig. 19) that was deflected downward approximately 24° relative to the "wing" targets. The spacing, size of the targets, and location of the target fixture in the test section were chosen to closely match an actual measurement on the LE slat of a research model. The target fixture was mounted on a tripod with a pivoting head to vary the angle of the fixture approximately along the direction of the LE. The fixture was tilted toward the model body from 0° to −10° to simulate an angular change that might occur for the LE slat and main wing targets during aeroelastic loading. The maximum angular change of −10° was selected to exaggerate the effect and is probably two to three times larger than typically expected. Images were acquired at each angle with a charge-coupled device (CCD) video data camera mounted on the test section wall normally used for deformation measurements at the facility. At each tilt angle, five sets of data were taken for later averaging. Repeat data sets were taken at 0°, −2°,−3° and −6°. Standard image processing and single-camera photogrammetry data reduction procedures used at the facility were applied to the imagery. The angle of the simulated control surface was fixed in relation to the main wing targets throughout the test. Any apparent change in the angle between the control surface and wing as the overall tilt angle of the fixture is varied is a measure of the error.

The errors in the control surface and main wing target angles after image processing, averaging, and data reduction are shown in figure 20. Each data point represents the average of five recordings with repeat data points at 0°, −2, −3°, and −6°. The angular error for the pair of targets on the "LE control surface" is nearly linear and reaches −4.52° at a tilt of −10°. The angular error for the pair of targets on the "main wing" is essentially at noise level, having a mean of 0.021° and a standard deviation of 0.022°, with a maximum variation of 0.064°. Note the similarity in functional form to the simulated data plots of figure 16. The general trends are very similar, although the magnitude of the angular error for the "LE control surface" for the tilt angle test at the NTF is less than the theoretical simulations (−0.86° compared to −1.31° at $\omega = -2°$). The apparent changes in lengths between targets 1, 2, 3, and 4 are presented in figure 21. The figure 22 data have similar trends compared to the simulated data plots depicted in figure 16, but the magnitude is a little greater (−0.022 in. compared to −0.017 in. at $\omega = -2°$ for the length between targets 1 and 4).

The angular data were corrected by two procedures. The first procedure used only the Y_{shift} based on a constant length of the target pair on the "LE control surface." The second procedure used additionally the Y_{shift} based on the "main wing." The shifts in Y of target 2 (LE control surface) and target 3 (main wing) to minimize the differences in lengths compared to their lengths at $\omega = 0°$ are presented in figure 22. With the sign convention used here, a positive Y value is directed toward the model body, which is the direction expected since the target fixture was tilted toward the body. The shift in Y for target 2 on the control surface is positive, indicating a tilt toward the body as expected; however, the shift in Y for target 3 is the opposite sign, which may be due to experimental error associated with the alignment of the target fixture to duplicate the measurement of the model LE slat. However, the overall correction is improved more by using the shift in both targets 2 and 3 rather than just target 2, as indicated in figure 23. The residual error is positive, indicating an overcorrection. Approximately 78 percent of the error is corrected when using only the shift in Y from target 2. Approximately 86 percent of the error is corrected when using the shifts in Y of targets 2 and 3. Thus, the controlled tilt angle experiment at the NTF roughly validates the error model mentioned previously and shows the value of the new correction procedure on real data with the geometry and camera actually used for deformation measurements on control surface.

LE Slat Angular Error and Correction During Wind-On Testing at NTF

Questionable LE slat angular deformation data during wind-on testing at the NTF prompted the effort reported here. Initially the uncorrected slat deformation data at an outboard semispan location during a recent test indicated a downward deflection of over 1° as positive aeroelastic loading occurred. This physically suspect result, coupled with an inboard slat measurement that showed very little deformation, prompted this investigation of bias errors that might cause such a result, while at the same time causing little error to main wing data. The reduced data for the angular deformation of the LE slat data (outboard location) for a series of runs at constant pitch angle during noncryogenic testing at the NTF and its subsequent correction are presented as a function of normalized dynamic pressure q in figure 24. The uncorrected data, which erroneously indicate a physically unlikely downward deflection of the control surface for positive wing loading, are indicated with circles. The corrected data are indicated with squares. After correction, the angular deformation data show little more than measurement noise level, indicating very little deformation of the LE slat during noncryogenic testing. The mean of the corrected data is −0.003°, with a standard deviation of 0.126°, which is considered close to the noise level of the measurements under wind-on conditions. The values of the spanwise tilt angle ω of the targets, computed from the values of Y_{shift} calculated from the correction procedure versus Z, are plotted versus normalized dynamic pressure q in figure 25. The plot is consistent with an increase in spanwise tilt angle as the localized bending increases due to higher aeroelastic loading.

Concluding Remarks

The single-camera photogrammetric bias error due to wing bending is much greater for control surfaces with large deflection angles to the main wing than for the main wing element. While typically the bias error due to bending for the main wing element is less than 0.05°, making correction for the main wing a minor concern, the bias error for control surfaces can exceed 1°. The bias error increases with the amount of bending and the magnitude of the initially set deflection angle of the control surface. A correction procedure based on the invariance of the length between targets can be used to estimate the shift in the Y coordinate used as reference in the photogrammetric computation for control surfaces, thus improving the computation of X and Z coordinates and hence the angle computations. Simulations indicate that corrections to about 2 percent of the error (98 percent of error removed) are possible with exact image plane coordinates and camera parameters. A controlled wind-off experimental test with typical measurement geometry indicates that a correction to about 15 percent of the error is possible, which for angular errors less than 1.3° would be about 0.2°.

References

1. Burner, A. W.; and Liu, Tianshu: Videogrammetric Model Deformation Measurement Technique. *J. of Aircr.*, vol. 38, no. 4, July/August 2001, pp. 745–754.

2. Burner, Alpheus W.; Wahls, Richard A.; and Goad, William K.: *Wing Twist Measurements at the National Transonic Facility*. NASA TM 110229, 1996.

3. Burner, A. W.; Liu, T.; and DeLoach, R.: Uncertainty of Videogrammetric Techniques Used for Aerodynamic Testing. *22nd AIAA Aerodynamic Measurement Technology and Ground Testing Conference*, St. Louis, Missouri, AIAA 2002-2794, June 24–26, 2002, p. 20.

4. Weisstein, Eric W.: Arc Length. From *MathWorld*—A Wolfram Web Resource. http://mathworld.wolfram.com/ArcLength.html. Accessed Jan. 4, 2005.

Appendix A

Arc Length Computation in *YZ* Plane

Arc length s is defined (ref. 4) as the length along the arc of a curve in three-dimensional (3-D) space. It is convenient for the case of bending in the YZ plane to consider the curve $f(Y)$ representing the bending to be expressed in vector form as the position vector from the origin

$$\vec{r}(Y) = Y\,\hat{Y} + f(Y)\,\hat{Z} \tag{A1}$$

where $\hat{Y}$ and $\hat{Z}$ are unit vectors along the Y and Z axes. Then, from reference 4, the arc length s can be shown to be given by

$$s = \int_a^b \sqrt{1 + f'^2(Y)}\, dY \tag{A2}$$

where $f'^2(Y)$ is the square of the derivative with respect to Y. The integrand of equation (A2) can be thought of as a differential form of the Pythagorean Theorem for finding the differential arc length ds as the hypotenuse of a right triangle with one leg of the right triangle given by dY and the other leg given by $dY \times$ slope, or $dY \times f'(Y)$. For second-order bending, for example with $a = 0$, $b = Y_1$, $f(Y) = CY_2$, and $f(Y) = 2CY$, the arc length s is given by equation (A3).

$$s = \int_0^{Y_1} \sqrt{1 + 4C^2Y^2}\, dY \tag{A3}$$

For first-, third-, and fourth-order bending, the term $4C^2Y^2$ in equation (A3) is replaced with C^2, $9C^2Y^4$, or $16C^2Y^6$, respectively. The problem is then to find Y_1 to maintain a constant arc length equal to the original Y location of the target as the bending occurs. Before bending occurs, the arc length s is the correct value of Y to use in the single-camera photogrammetric computation. As bending occurs, the Y shift, ΔY, of a target is given by $s - Y_1$, where Y_1 must be found to maintain the arc length constraint. Equation (A3) can be evaluated numerically or, for simple cases like linear and second-order bending, explicitly. For example, equation (A3) for second-order bending can be evaluated to yield

$$s = \frac{2CY_1\sqrt{1 + 4C^2Y_1^2} + \sinh^{-1}\left(2CY_1\right)}{4C} \tag{A4}$$

A useful approximation to the expression for ΔY for second-order bending is (ref. 3)

$$s - Y_1 = \Delta Y \approx \frac{2}{3}C^2Y^3 \tag{A5}$$

For typical wing tip deflection values of less than the 1 in. experienced in transonic testing, the error in Y shift when using equation (A5) is less than 0.0001 in. for a 30-in. semispan undergoing second-order bending, making equation (5A) a useful, quick approximation. For example, if $Y = 30$ in., $C = 1/900$ with a tip deflection of 1 in. based on $1 = CY^2$, so that $\Delta Y \approx 0.022$ in. from equation (A5). In other words, the correct Y to use for the deflected tip target should be less by this ΔY. A partial correction for this effect can be implemented by first calculating the X, Z coordinates without correction for ΔY, and then by determining a first estimate of C for use in equation (A5) to get an estimate of the correction ΔY to apply before recomputing X, Z with the single-camera solution. One or two iterations should be sufficient for typical applications. A limitation of this correction technique is that the functional form of the bending must be known as well as the location of zero bending.

Appendix B

Single-Camera Photogrammetry Solution

The single-camera photogrammetry solution is derived from the collinearity equations (ref. 3), which are the most fundamental and important data reduction equations in photogrammetry. The collinearity equations express the relationship that the object point, perspective center, and image point lie on a straight line.

$$
\begin{aligned}
x &= x_p - c\left[\frac{m_{11}\left(X-X_c\right)+m_{12}\left(Y-Y_c\right)+m_{13}\left(Z-Z_c\right)}{m_{31}\left(X-X_c\right)+m_{32}\left(Y-Y_c\right)+m_{33}\left(Z-Z_c\right)}\right] \\
y &= y_p - c\left[\frac{m_{21}\left(X-X_c\right)+m_{22}\left(Y-Y_c\right)+m_{23}\left(Z-Z_c\right)}{m_{31}\left(X-X_c\right)+m_{32}\left(Y-Y_c\right)+m_{33}\left(Z-Z_c\right)}\right]
\end{aligned} \tag{B1}
$$

In equation (B1) the image coordinates *x, y* have been corrected for optical lens distortion. The photogrammetric principal point is represented by x_p, y_p, the principal distance is represented by *c*, and the object space location is represented by *X, Y, Z*. The location of the perspective center is represented by X_c, Y_c, Z_c. The Euler angles ω, ϕ, κ, which orient the image plane to the coordinate system of interest about the *X*, *Y*, *Z* axes, respectively, are used to compute the nine elements of the rotation matrix given by equation (B2).

$$
\begin{aligned}
m_{11} &= \cos\phi\cos\kappa \\
m_{12} &= \sin\omega\sin\phi\cos\kappa+\cos\omega\sin\kappa \\
m_{13} &= -\cos\omega\sin\phi\cos\kappa+\sin\omega\sin\kappa \\
m_{21} &= -\cos\phi\sin\kappa \\
m_{22} &= -\sin\omega\sin\phi\sin\kappa+\cos\omega\cos\kappa \\
m_{23} &= \cos\omega\sin\phi\sin\kappa+\sin\omega\cos\kappa \\
m_{31} &= \sin\phi \\
m_{32} &= -\sin\omega\cos\phi \\
m_{33} &= \cos\omega\cos\phi
\end{aligned} \tag{B2}
$$

Consider a target location *X*, *Y*, *Z* where *X* is in the flow direction, *Y* is along the wing span, and *Z* is up. If one of the spatial coordinates, such as *Y*, is known, then a single camera image of a point results in two equations in two unknowns. With *Y* known, *X* and *Z* can be found from

$$
\begin{aligned}
X &= X_c + \frac{\left(Y-Y_c\right)\left(a_2a_6-a_5a_3\right)}{a_4a_3-a_1a_6} \\
Z &= Z_c - \frac{\left(X-X_c\right)a_1+\left(Y-Y_c\right)a_2}{a_3}
\end{aligned} \tag{B3}
$$

where

$$\begin{aligned}
a_1 &= \left(x - x_p\right) m_{31} + c\, m_{11} \\
a_2 &= \left(x - x_p\right) m_{32} + c\, m_{12} \\
a_3 &= \left(x - x_p\right) m_{33} + c\, m_{13} \\
a_4 &= \left(y - y_p\right) m_{31} + c\, m_{21} \\
a_5 &= \left(y - y_p\right) m_{32} + c\, m_{22} \\
a_6 &= \left(y - y_p\right) m_{33} + c\, m_{23}
\end{aligned} \tag{B4}$$

Once the X and Z coordinates are computed for a given semispan location, a slope angle is computed in the XZ plane by either least squares, or directly when there are only two targets per semispan. This angle, designated as the raw videogrammetric angle θ_{raw}, is given at each semispan η by equation (B5). The sign of this angle is usually inverted so that positive angles indicate leading edge (LE) up (for X in the flow direction and Z up).

$$\theta_{raw}\left(\eta\right) = \tan^{-1} \frac{\Delta Z_\eta}{\Delta X_\eta} \tag{B5}$$

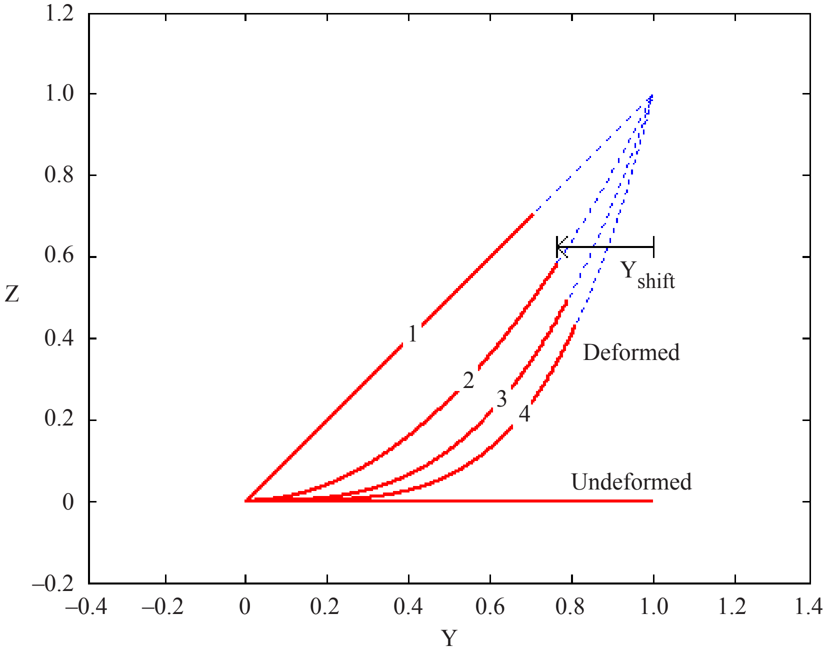

Figure 1. Shift in Y coordinate for deformation of order 1 to 4 with constraint of length = unity (Y_{shift} at tip for second-order bending is indicated).

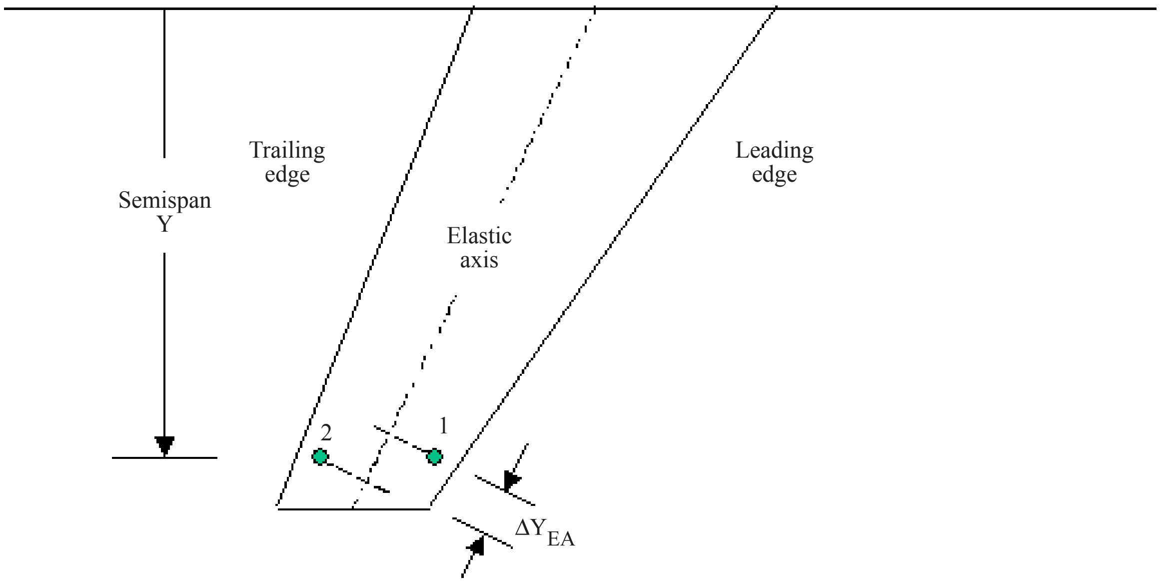

Figure 2. Two targets with same semispan Y but separated along elastic axis by ΔY_{EA}. Target 1 is nearest leading edge. Target 2 is nearest trailing edge.

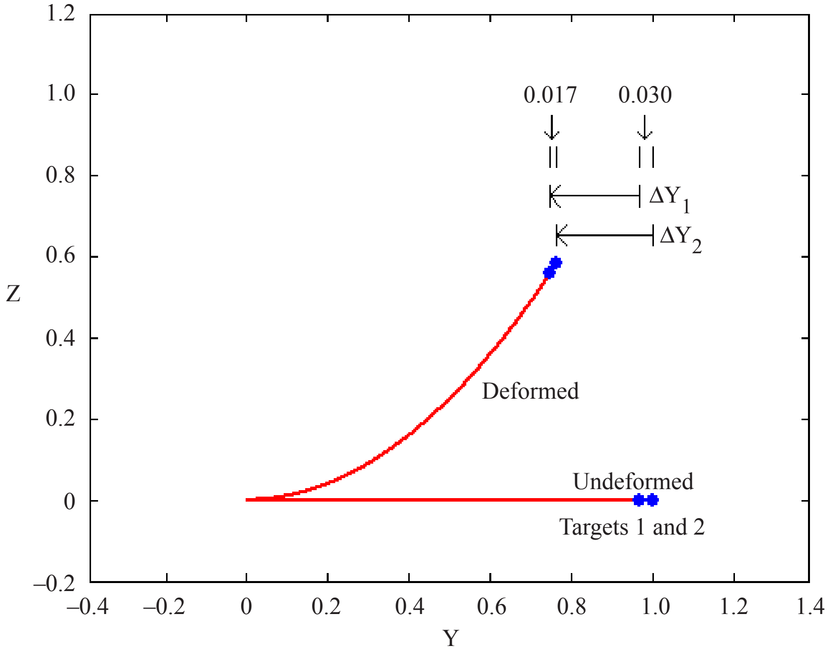

Figure 3. Shifts in *Y* coordinate of leading-edge (1) and trailing-edge (2) targets undergoing second-order wing bending illustrating initial *Y* separation of 0.030 and separation after bending of 0.017.

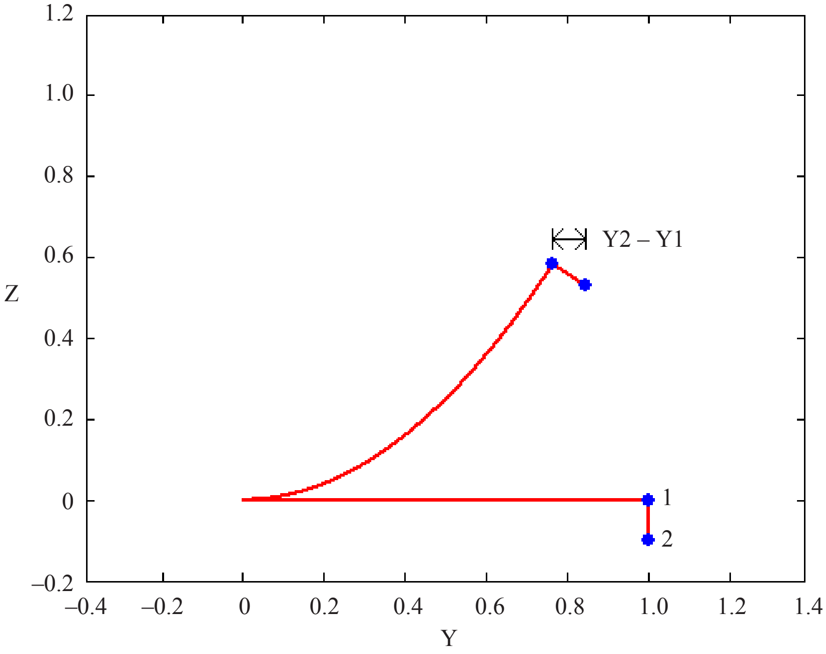

Figure 4. Difference in *Y* coordinates of control surface targets when undergoing second-order wing bending.

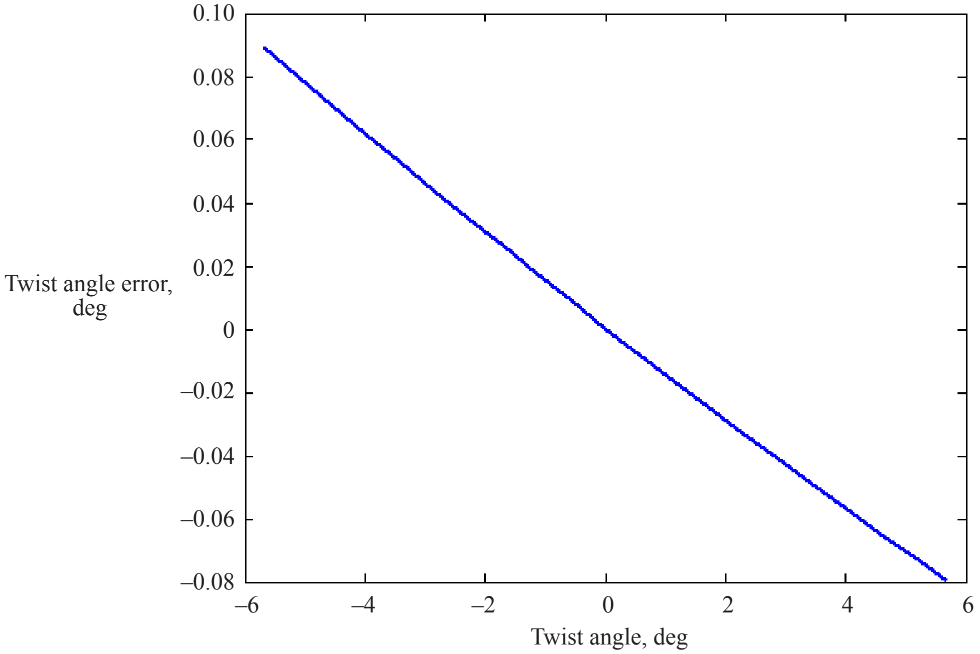

Figure 5. Twist angle error due to second-order bending versus known twist angle for the National Transonic Facility (NTF) geometry simulation.

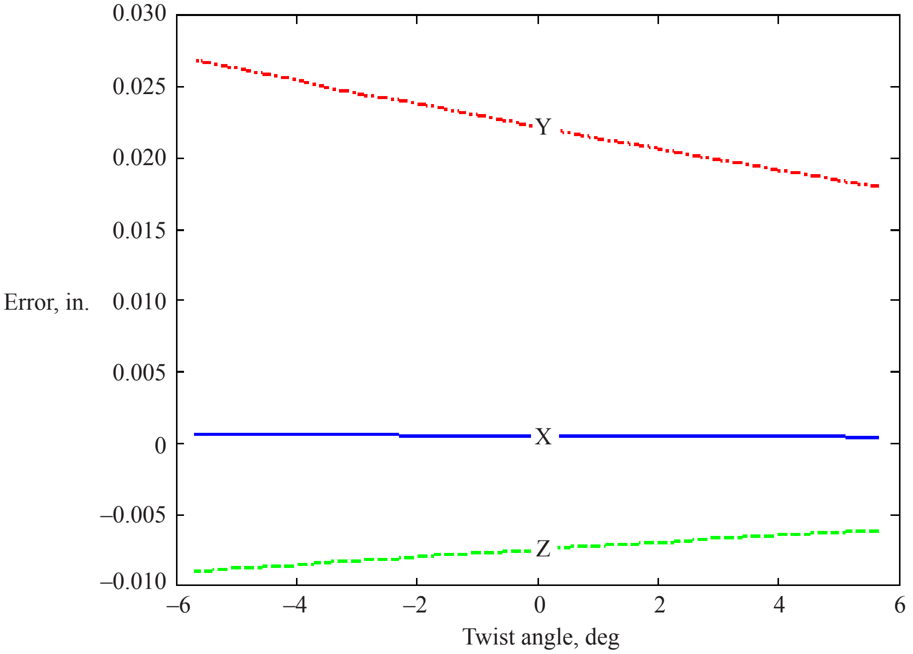

Figure 6. Error in X, Y, and Z due to second-order bending versus known twist angle for NTF geometry simulation.

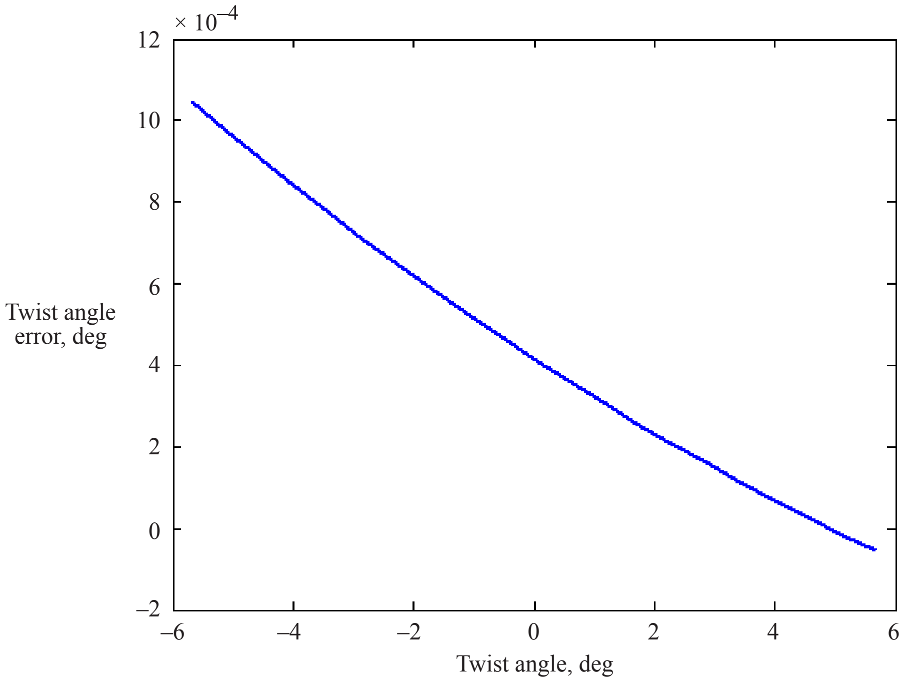

Figure 7. Error in twist angle after iterative correction procedure for *Y* versus known twist angle for NTF geometry simulation.

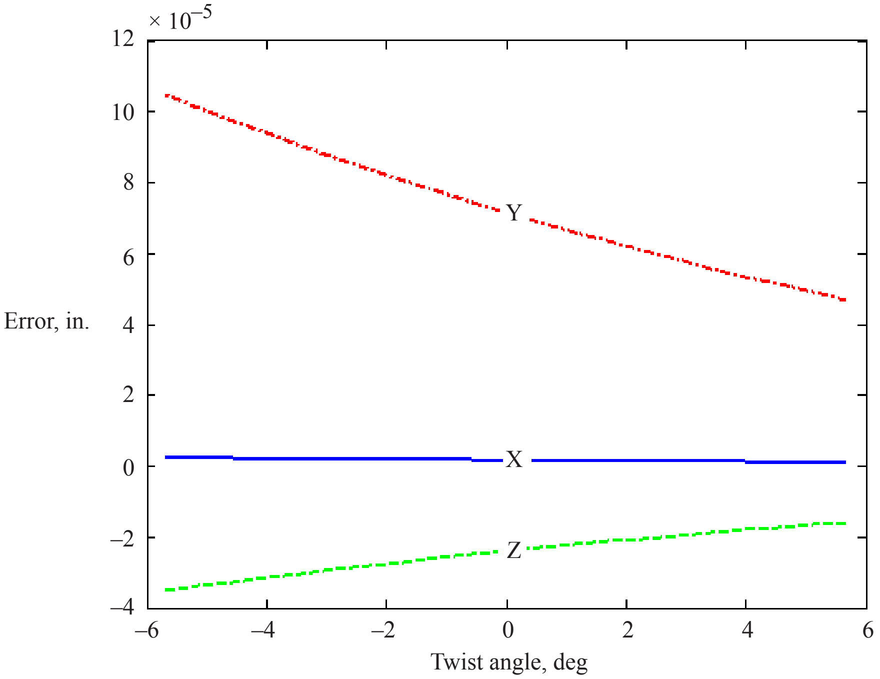

Figure 8. Error in *X*, *Y*, and *Z* after iterative correction procedure for Y versus known twist angle for NTF geometry simulation.

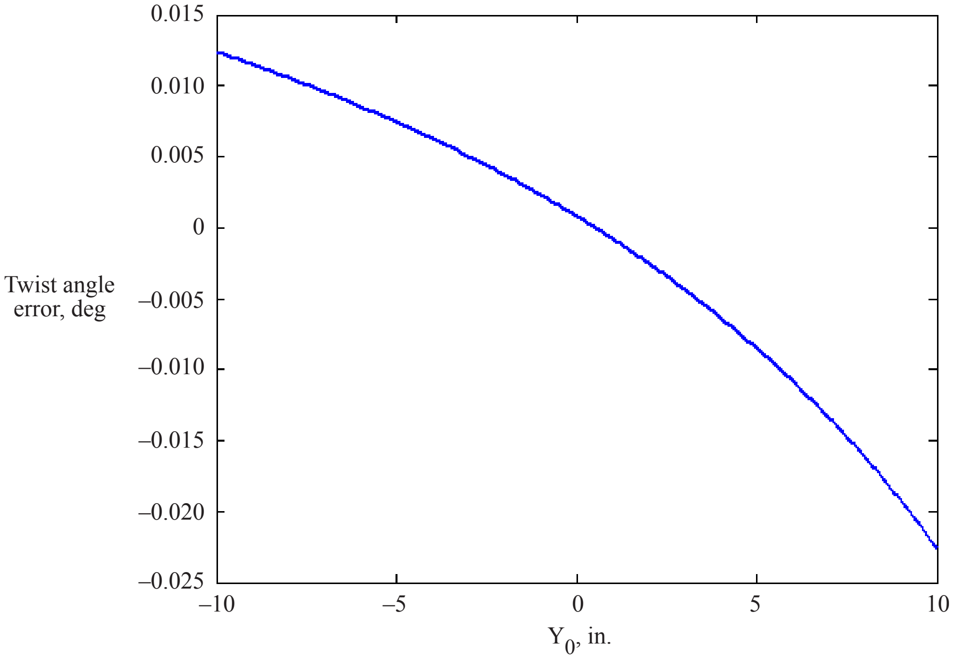

Figure 9. Error in 3° twist angle versus error in Y_o for NTF geometry simulation.

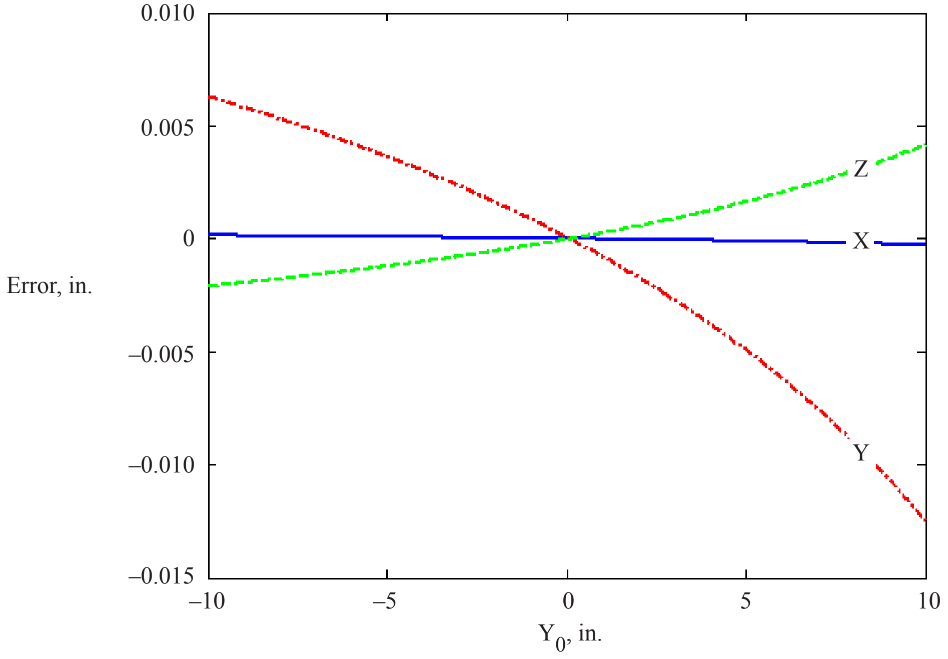

Figure 10. Error in X, Y, and Z for twist angle of 3° versus Y_o for NTF geometry simulation.

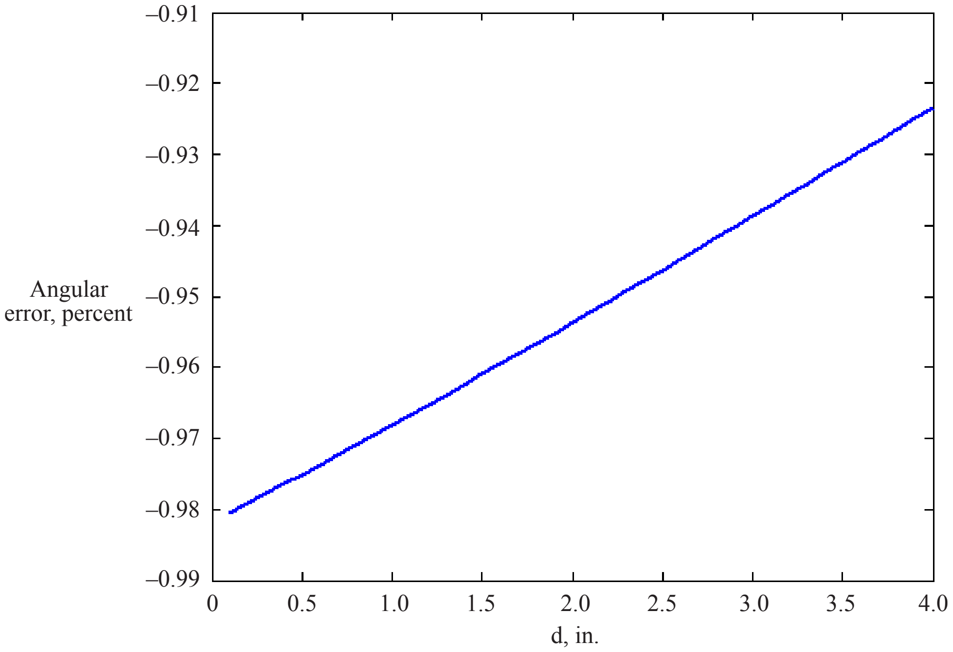

Figure 11. Angular error in percent versus target spacing *d* for a 30° rearward swept wing at semispan of 30 in. (with a corresponding variation of twist from 0° to −6°).

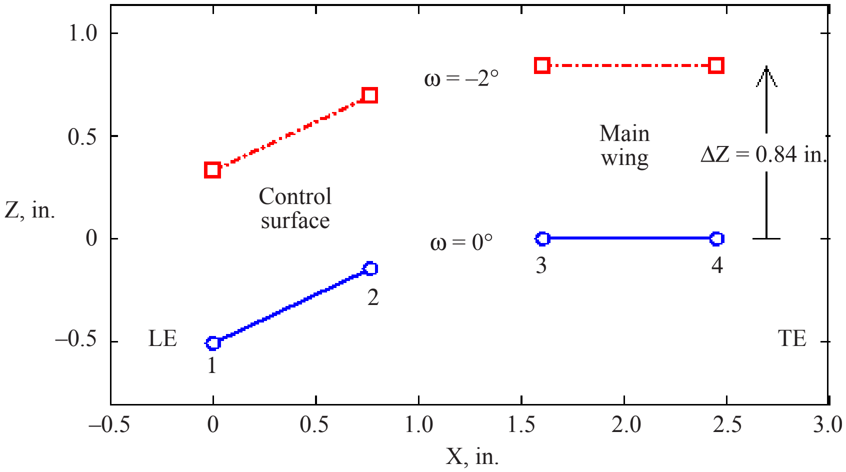

Figure 12. Target locations in *XZ* plane for bending error simulation before (ω = 0°, circles) and after (ω = −2°, squares) the maximum upward linear bending occurs. The LE control surface is set at −25°. Flow is from left to right. Target 1 is nearest the leading edge (LE) and target 4 is nearest the trailing edge (TE).

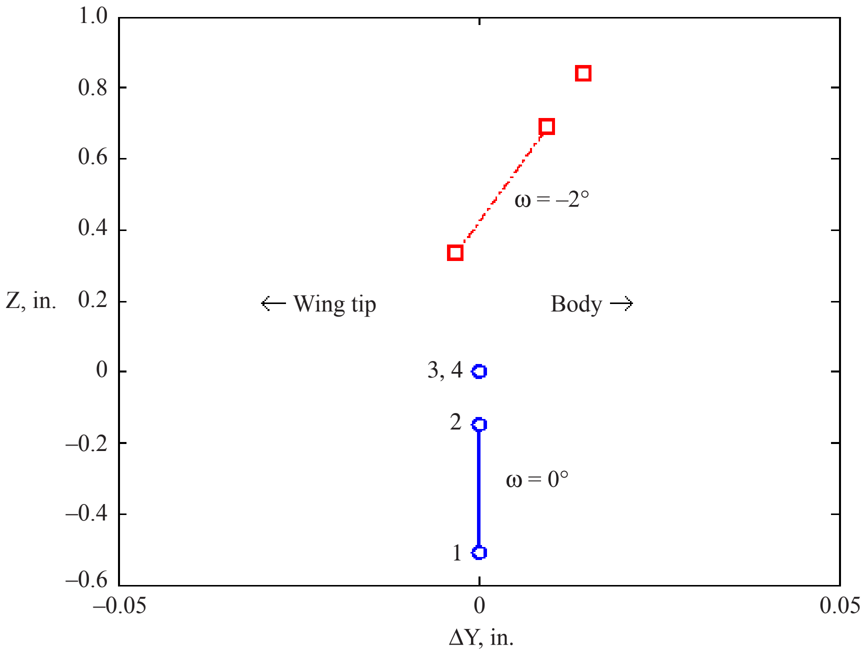

Figure 13. Shift in Y of 4 targets located 24 in. from center of rotation as linear bending occurs from 0° to a maximum of –2°.

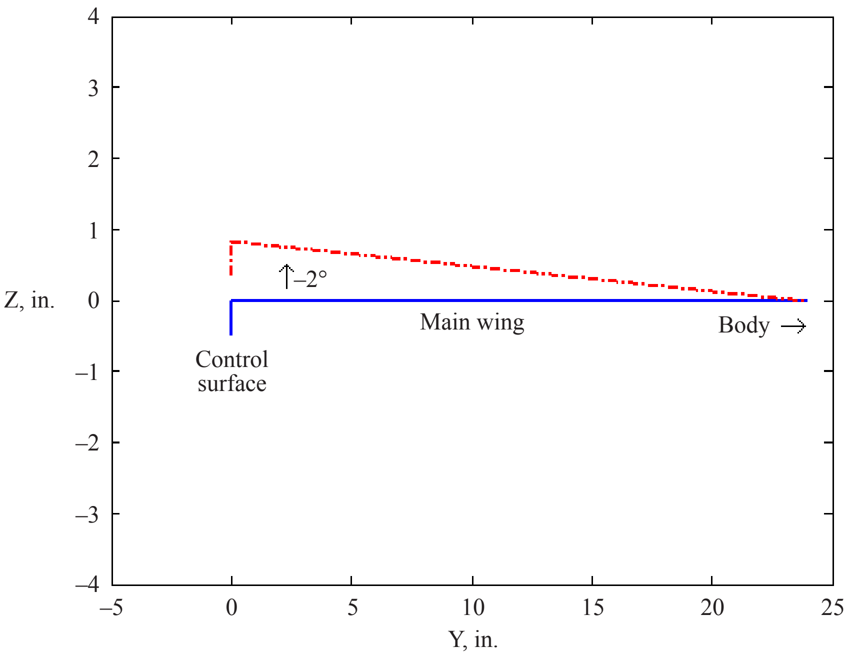

Figure 14. Illustration of linear bending in spanwise direction used for simulation.

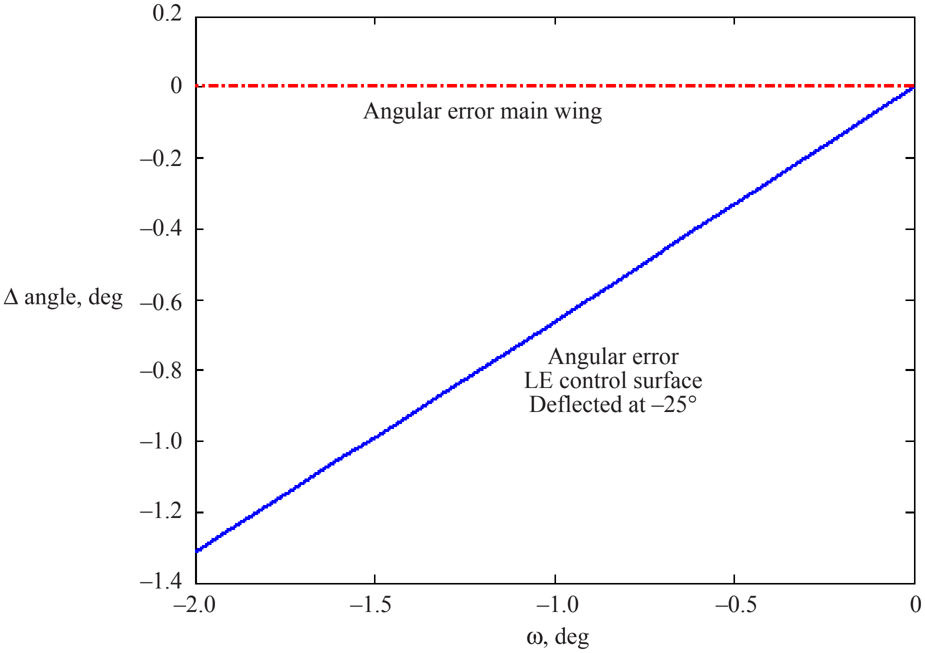

Figure 15. Angular error for main wing and LE control surface set at –25° as a function of linear bending.

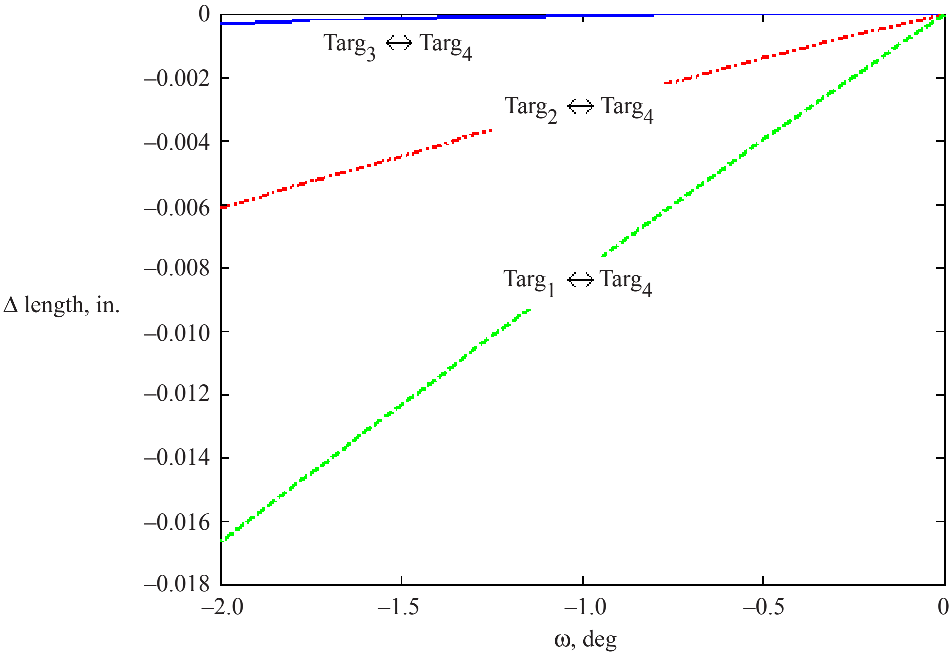

Figure 16. Error in lengths between targets 1, 2, 3, and 4 for LE control surface simulation undergoing linear bending. Targets 1 and 2 are on control surface. Targets 3 and 4 are on main wing.

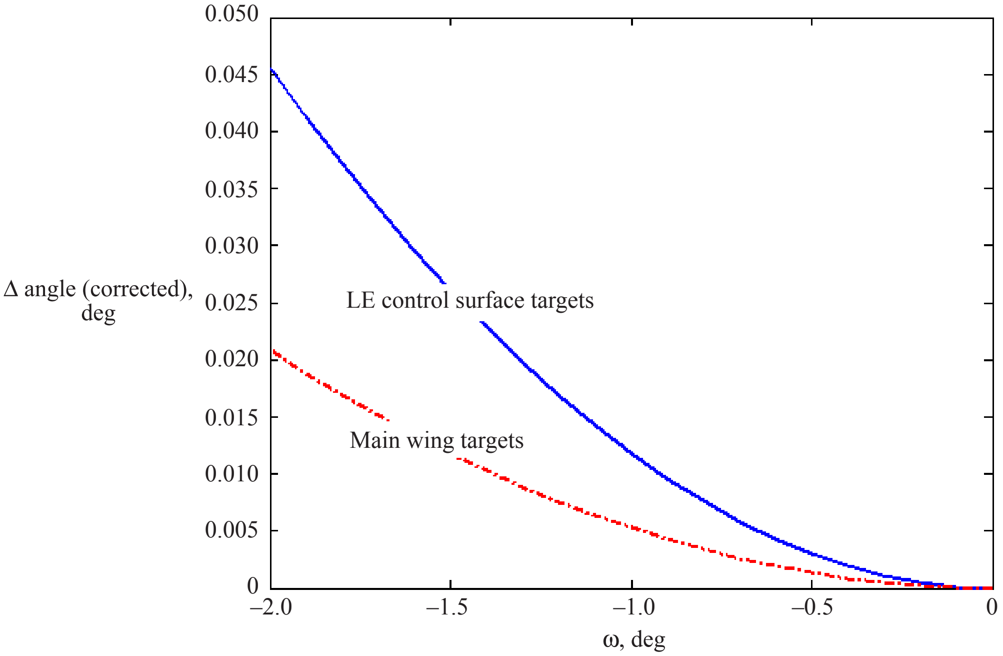

Figure 17. Residual errors in control surface and main wing angles after correction for *Y* shift.

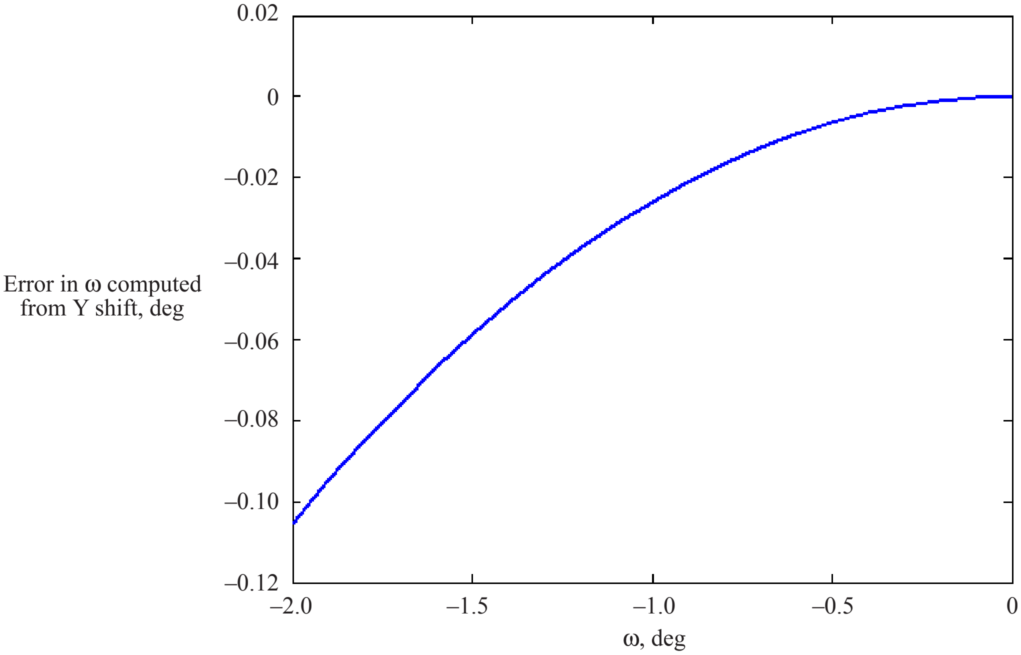

Figure 18. Error in ω from *Y*-shift correction procedure.

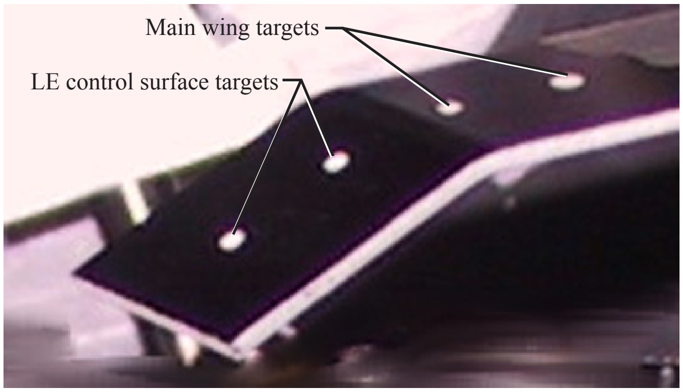

Figure 19. Fixture used to simulate LE control surface and main wing targets during wind-off angle test at NTF.

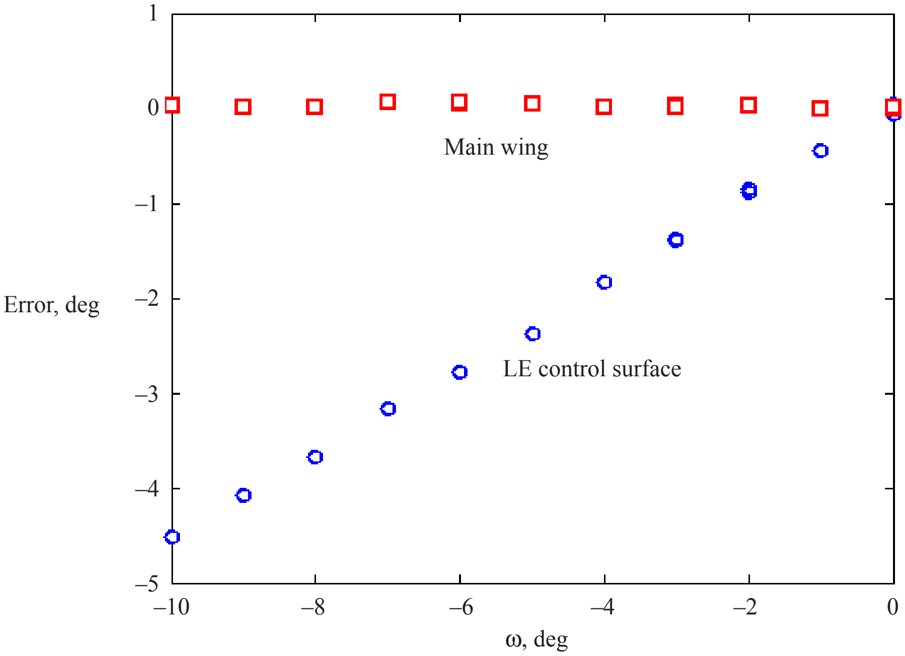

Figure 20. Angular error in main wing and LE control surface target pairs on fixture from wind-off angle test at NTF test section.

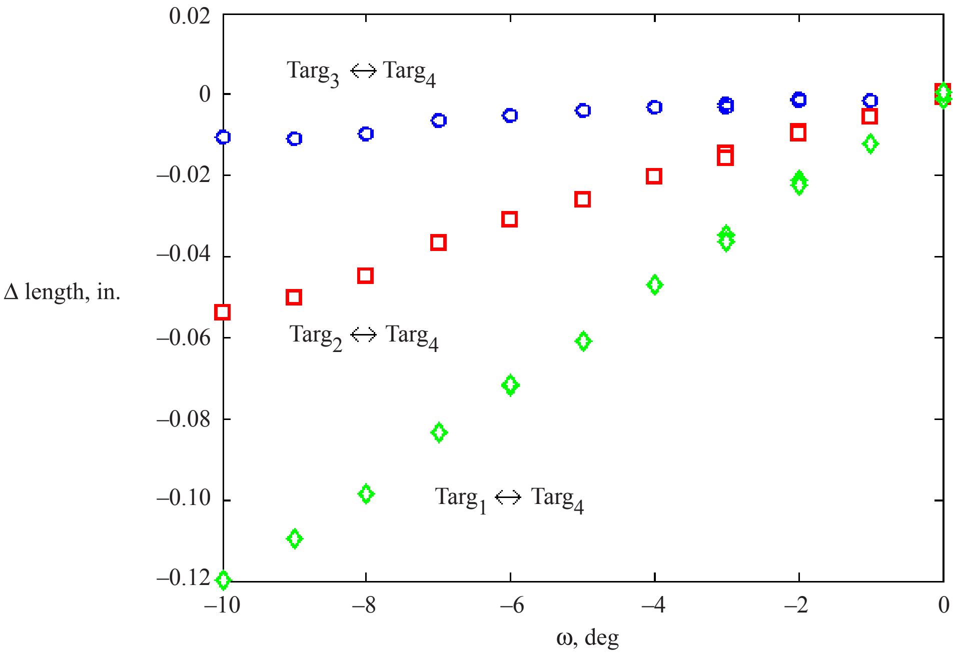

Figure 21. Apparent change in lengths between target pairs for tilt angle test at NTF.

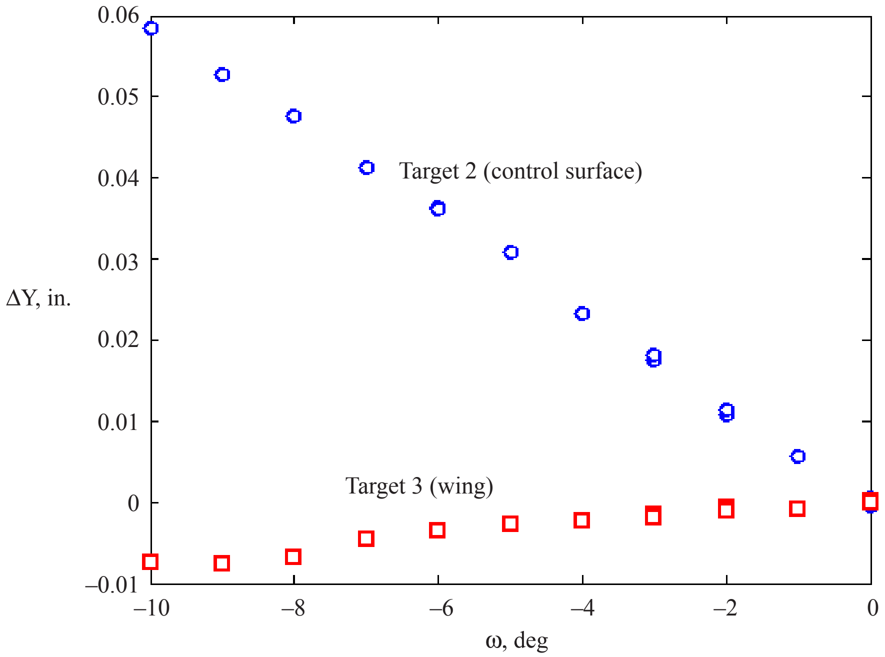

Figure 22. Shift in Y of targets 2 and 3 to minimize differences in lengths between target pairs 1 ↔ 2 and 3 ↔ 4 compared to their length at ω = 0°.

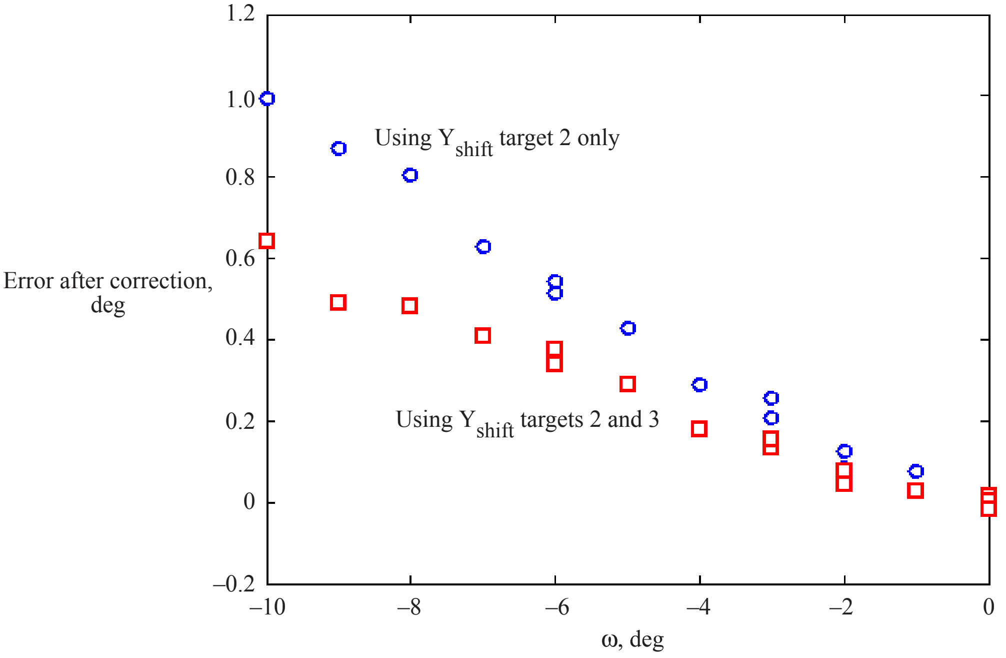

Figure 23. Residual error after correction using Y_{shift} from just target 2 (circles) and Y_{shift} from targets 2 and 3 (squares).

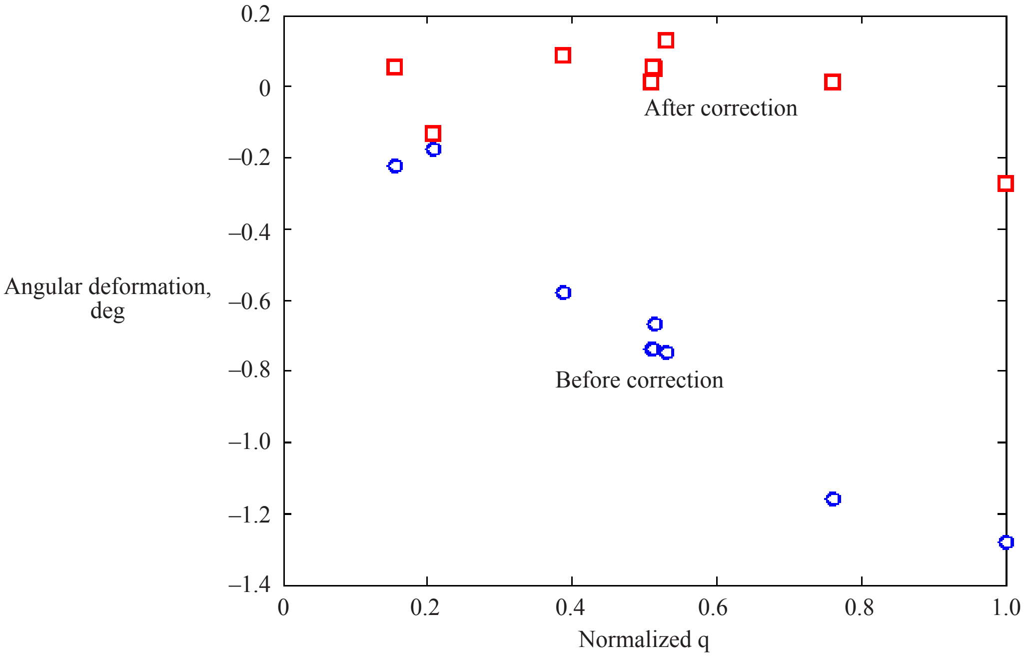

Figure 24. Angular deformation of LE slat subject to aeroelastic loading during noncryogenic testing at NTF versus normalized dynamic pressure q before (circles) and after correction for bending error (squares).

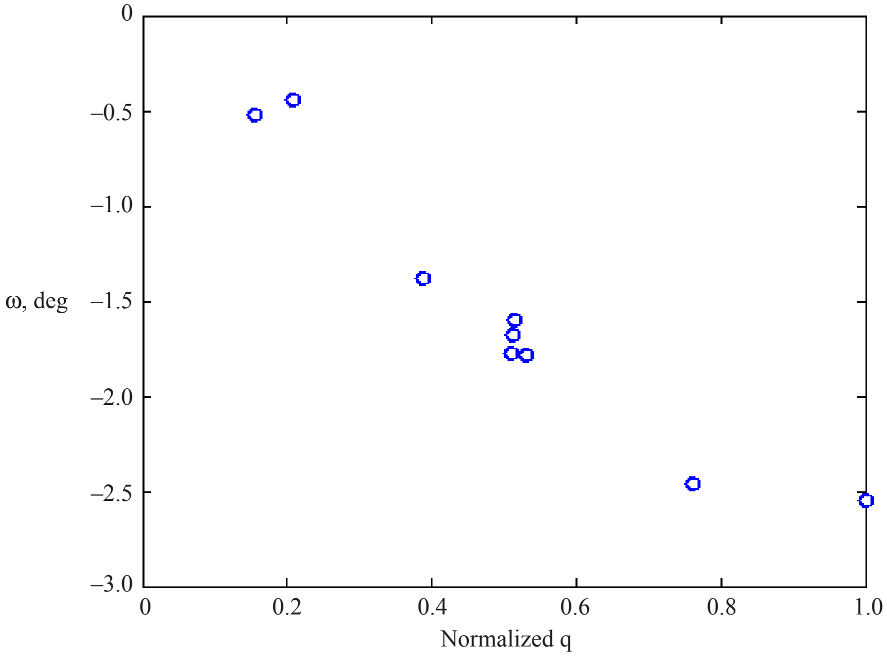

Figure 25. Computed ω based on the Y_{shift} values from the correction procedure for noncryogenic runs at NTF.

REPORT DOCUMENTATION PAGE	*Form Approved* *OMB No. 0704-0188*

1. REPORT DATE *(DD-MM-YYYY)* 01- 05 - 2005	**2. REPORT TYPE** Technical Memorandum	**3. DATES COVERED** *(From - To)*

4. TITLE AND SUBTITLE Error Due to Wing Bending in Single-Camera Photogrammetric Technique	**5a. CONTRACT NUMBER**
	5b. GRANT NUMBER
	5c. PROGRAM ELEMENT NUMBER
6. AUTHOR(S) Burner, Alpheus W., Jr.; and Barrows, Danny A.	**5d. PROJECT NUMBER**
	5e. TASK NUMBER
	5f. WORK UNIT NUMBER 23-090-80-40

7. PERFORMING ORGANIZATION NAME(S) AND ADDRESS(ES) NASA Langley Research Center Hampton, VA 23681-2199	**8. PERFORMING ORGANIZATION REPORT NUMBER** L-19021
9. SPONSORING/MONITORING AGENCY NAME(S) AND ADDRESS(ES) National Aeronautics and Space Administration Washington, DC 20546-0001	**10. SPONSOR/MONITOR'S ACRONYM(S)** NASA
	11. SPONSOR/MONITOR'S REPORT NUMBER(S) NASA/TM-2005-213254

12. DISTRIBUTION/AVAILABILITY STATEMENT
Unclassified - Unlimited
Subject Category 35
Availability: NASA CASI (301) 621-0390

13. SUPPLEMENTARY NOTES
Burner and Barrows, Langley Research Center, Hampton, VA.
An electronic version can be found at http://ntrs.nasa.gov

14. ABSTRACT

The error due to wing bending introduced into single-camera photogrammetric computations used for the determination of wing twist or control surface angular deformation is described. It is shown that the error due to wing bending when determining main wing element-induced twist is typically less than 0.05° at the wing tip and may not warrant additional correction. It is also shown that the angular error in control surface deformation due to bending can be as large as 1° or more if the control surface is at a large deflection angle compared to the main wing element. A correction procedure suitable for control surface measurements is presented. Simulations of the error based on typical wind tunnel measurement geometry, and results from a controlled experimental test in the test section of the National Transonic Facility (NTF) are presented to confirm the validity of the method used for correction of control surface photogrammetric deformation data. An example of a leading edge (LE) slat measurement is presented to illustrate the error due to wing bending and its correction.

15. SUBJECT TERMS
Control surfaces; Deformation; Photogrammetry; Wings

16. SECURITY CLASSIFICATION OF:			**17. LIMITATION OF ABSTRACT**	**18. NUMBER OF PAGES**	**19a. NAME OF RESPONSIBLE PERSON**
a. REPORT	**b. ABSTRACT**	**c. THIS PAGE**			STI Help Desk (email: help@sti.nasa.gov)
					19b. TELEPHONE NUMBER *(Include area code)*
U	U	U	UU	31	(301) 621-0390